Inter-Percentile Velocity Width: An Alternative Parametrization of the Velocity Field of the Broad-Line Region

A Senior Honors Thesis

Presented in Partial Fulfillment of the Requirements for Graduation with Distinction in Astronomy in the Undergraduate College of Arts and Sciences of The Ohio State University

By

Mallory E. Molina

The Ohio State University

May 2012

Project Adviser: Professor Bradley Peterson

Inter-Percentile Velocity Width: An Alternative Parametrization of the Velocity Field of the Broad-Line Region

Mallory E. Molina
Department of Astronomy, The Ohio State University
140 West 18th Avenue, Columbus, OH 43210-1173

ABSTRACT

In this project we compare an alternative parametrization of gas motions near supermassive black holes in active galactic nuclei (AGN) with other common parametrizations to see which best characterizes these motions and leads to accurate measurements of central black hole masses. Two parametrizations that are widely used for characterizing the widths of spectral emission lines are line dispersion (σ_{line}) and full width at half maximum (FWHM). This project involves writing the computer code for and testing an alternative parametrization, the inter-percentile velocity (IPV) width. The IPV is designed to avoid problems that affect the other parameters, principally noise with FWHM and blending with other features with σ_{line}, and hopefully retain the positive aspects. The ultimate goal is to develop a simple prescription for accurate measurements of black hole masses under a wide variety of conditions.

1. INTRODUCTION

Active galactic nuclei (AGNs) are the dense luminous central cores of galaxies that can radiate more than all the stars in the entire galaxy. The central core is comprised of a supermassive black hole, typically of mass $10^6 M_\odot$ to $10^9 M_\odot$, and surrounding material. The material that actively accretes onto the central black hole forms a structure called the accretion disk. The accretion disk creates continuum radiation that excites lower density gas further out in the galactic nucleus. This excited gas then creates the emission lines that are prominent spectral features of AGNs. The material is accelerated by the gravitational force of the black hole, giving the gas high Doppler motions. These motions broaden the emission lines to order of 1000 to 10,000 km s^{-1}, so this emission is said to arise in the "broad-line region" (BLR).

The masses of the central black holes in some AGN can be calculated using a technique called reverberation mapping. Reverberation mapping is a technique that measures the response of emission lines to variation in the continuum radiation from the accretion disk. The emission line response to the change in continuum flux is delayed due to light travel time effects (Blandford and McKee 1982). This delay is called the time lag τ, and when multiplied by the speed of light, can be used to approximate the radius of the BLR.

The measurement of time lag that this project will use is τ_{cent}, which is the mean of the "cross-correlation centroid distribution" (Maoz & Netzer 1989; Peterson et al. 2004). For our purposes, it

is only necessary to know that the τ_{cent} is based on the centroid of the distribution, whereas τ_{peak} is based on the peak of the distribution. Both of these time-lag measurements are useful, but for consistency with other work, we will concentrate on τ_{cent}.

If the BLR gas motions around the central source, or black hole, are gravitationally dominated, the virial theorem applies. The mass of the central black hole is then given by

$$M = \frac{f c\tau \Delta V^2}{G} \tag{1}$$

where ΔV is a velocity dispersion, $c\tau$ is the radius of the BLR, f is a constant of order unity that depends on the geometry of the BLR. This mass is called the virial product when $f = 1$; i.e. the virial product is based solely on the observables.

The velocity dispersion is measured by some simple parametrization of BLR emission lines. Currently there are two widely used parametrizations, line dispersion (σ_{line}) and full width at half maximum (FWHM). These parametrizations have merit, but both are affected by the contamination of the pure broad line profile by other spectral features (Peterson et a1. 2004). For this project, we test a new parametrization, the inter-percentile velocity (IPV). The IPV parametrization is designed to avoid problems that affect the other two parameters and to retain the positive aspects of both previous parametrizations. We will first test its consistency with the virial relationship by plotting it against the time lag. We will then look at the bias of the parametrization in terms of blended spectral features in Hβ.

2. PREVIOUS PARAMETRIZATION METHODS

For a given emission line profile, $P(\lambda)$, we can currently parametrize the line width two different ways: σ_{line} or FWHM, as discussed by Peterson et al. (2004).

The FWHM parametrization is computed differently depending on whether the emission line is single- or double- peaked. For a single-peaked emission line, the line peak $P(\lambda_{max})$ is identified. Then a search starting on the blue side of the line profile up to the peak searches for λ_1 such that $P(\lambda_1) = 0.5P(\lambda_{max})$. Then the search is repeated, this time from the line peak down the blue side of the profile to find λ_2 such that $P(\lambda_2) = 0.5P(\lambda_{max})$. The mean of these two wavelengths is taken as the wavelength at half maximum. This process is repeated on the red side of the profile, and the difference of these two wavelengths is taken to be the FWHM of the line profile. For a double-peaked emission line, we define the two peaks, $P(\lambda)_{max,short}$ and $P(\lambda)_{max,long}$. Then the process described above is repeated, this time finding the wavelength on the blue side of the line with respect to $P(\lambda)_{max,short}$ and the wavelength on the red side of the line with respect to $P(\lambda)_{max,long}$. The difference of those two wavelengths is then taken to be the FWHM of the line profile.

The line dispersion parametrization is less dependent on the shape of the profile. The first

moment of the line profile is

$$\lambda_0 = \int \lambda P(\lambda)\, d\lambda \Big/ \int P(\lambda)\, d\lambda. \tag{2}$$

The second moment of the profile is

$$\sigma^2_{line}(\lambda) = \langle \lambda^2 \rangle - \lambda_0^2 = \left[\int \lambda^2 P(\lambda)\, d\lambda \Big/ \int P(\lambda)\, d\lambda \right] - \lambda_0^2. \tag{3}$$

The line dispersion of the profile is the square root of this equation, σ_{line}.

Each of these parametrizations have strengths and weaknesses. FWHM is a trivial measurement, and can even be estimated graphically. Compared to σ_{line}, FWHM is not strongly affected by blending with other lines or extended line wings. However, narrow line contamination can lead to an underestimation of the line width. Conversely, σ_{line} is less sensitive to narrow components, but blending with other lines and extended line wings can lead to an overestimation of the line width. This is because σ_{line} weights the points on the profile according to the distance of that point from line center. This means that the extended line wings will have more weight than the central region of the line.

We are employing a new parametrization that is designed to reduce these problems. The IPV parametrization can effectively avoid issues with the wings, like FWHM, and evenly weights the flux contribution from all the points on the line profile. This reduces the problem with the extended wings, as well as the affect of narrow line contamination. Thus the IPV parametrization is designed to retain the positive aspects of the two previous parametrizations, and hopefully will mitigate the negative aspects.

3. INTER-PERCENTILE VELOCITY PARAMETRIZATION

We define $IPV(F)$ as the separation between the wavelengths λ_1 and λ_2 that contains the central $F\%$ of the flux in the emission line. The measurement is calculated by first integrating over the entire line profile to get the total flux. After this, the specified $F\%$ flux is used to determine two integrated fluxes, f_1 and f_2, which are defined relative to the total line flux such that

$$f_1 = \frac{1 - (F/100)}{2} \tag{4}$$

and

$$f_2 = 1 - f_1. \tag{5}$$

Thus, for the line profile, $P(\lambda)$, we can then calculate the IPV value by using the two endpoints on the integrals for f_1 and f_2, such that

$$f_1 = \int_{-\infty}^{\lambda_1} P(\lambda)\, d\lambda \tag{6}$$

and

$$f_2 = \int_{\lambda_2}^{\infty} P(\lambda)\, d\lambda. \tag{7}$$

After calculating the total flux, we search from the blue end of the line, and find the wavelength that corresponds to λ_1. We do this by integrating up from the endpoints on the curve from each side. Once we find two values that bound the desired wavelength, we linearly interpolate between the two to calculate the desired wavelength. We then search from the red end of the line up the profile and find the wavelength that corresponds to λ_2 using the same process. This will then give us the IPV width

$$IPV(F) = \lambda_2 - \lambda_1. \tag{8}$$

Thus $IPV(90)$ would give $f_1 = 0.05$, or that 5% of the flux is shortward of the limit λ_1, and $f_2 = 0.95$, so 5% of the flux is longward of the limit λ_2. When these two are subtracted, 90% of the flux is contained by λ_1 and λ_2, and $IPV(90) = \lambda_2 - \lambda_1$. From here, we can use the Doppler formula to convert to velocity, so that

$$IPV(90) = \frac{(\lambda_2 - \lambda_1)c}{\lambda_{rest}(1+z)} \tag{9}$$

where c is the speed of light, λ_{rest} is the rest wavelength of the emission line, and z is the red shift of the object.

We have written a computer code to determine IPV widths for broad lines in AGN spectra, and we combined it with the code from Peterson et al. (2004). We therefore can simultaneously calculate IPV, σ_{line}, and FWHM widths. We test both the consistency of the parametrization with the virial relationship, as well as the bias of the parametrization in terms of blended spectra. The spectral emission line that we will focus on most is Hβ. We will look at several UV lines and Hβ in terms of the virial relationship, and only Hβ in terms of the bias of the parametrization.

4. Hβ REGION

The emission line most commonly used to measure the velocity dispersion of the BLR is Hβ. The Hβ line is a prominent emission line located in an easily accessible portion of the spectrum. The line is also very close to the forbidden lines [OIII]λ4959,5007. These lines do not vary and thus can be used for flux calibration, which ensures the accuracy of the continuum and broad line flux variations. This makes Hβ a clear choice for a good spectral line to use to measure the velocity dispersion.

The problem with using the Hβ emission line is that the spectral region in which it lies is complicated. Hβ has a narrow line component, as well as an "FeII shelf" on the red side of the line. The forbidden lines [OIII]λ4959,5007 may also actually be on the BLR emission line itself. The equivalent width of the FeII emission and the FWHM(Hβ) are related, and the FeII affects the shape of the line, which is very important for the accuracy of the parametrization methods

(Boroson and Green 1992). Another important point is that the FeII emission that blends with the Hβ lines vary over time scales that are long compared to reverberation time scales (Vestergaard & Peterson 2005). This means that while the FeII emission does *vary*, it does not *reverberate*. This is an important distinction for the FeII emission, as it is not as easy to subtract from the spectra as the [OIII]λ4959,5007 lines are.

While Hβ is the most important emission line for reverberation studies, we also examine the UV lines SiIVλ1400, CIVλ1549, HeIIλ1640, and CIII]λ1909 to check for consistency with the virial relationship for the three parametrizations. These lines are a subset of the emission lines used by Peterson et al. (2004).

5. DATA

The data used in this investigation are a homogeneous subset of the spectra of the Seyfert 1 galaxy NGC 5548 from the International AGN Watch data base. These were obtained over many years, during which large variations in flux, time lags, and line profiles were observed. Our basic premise is that irrespective of these variations, our method should always yield the same black hole mass. We looked at both the root mean square residual spectrum (rms spectra) and mean spectra for each of these data sets. The difference between the rms and mean spectra is how the spectra in each set is averaged over. The mean spectra is calculated by averaging the value of the flux at each individual wavelength for all wavelengths. The rms spectra is the average squared deviation from the mean spectrum minus the square of the mean spectrum. This means that the rms spectrum is isolating the variable parts of the spectrum, so that anything constant will not appear.

6. RESULTS

The IPV parameter was tested for its accuracy in terms of the virial relationship, as well as the effects of blending, along with σ_{line} and FWHM.

6.1 Behavior of Inter-Percentile Velocity

We measured the widths-FWHM, σ_{line}, and IPV-of spectral lines in the rms and mean spectra constructed from thirteen years of Hβ data, and two years of observations of the UV lines SiIVλ1400, CIVλ1549, HeIIλ1640, and CIII]λ1909. We used a bootstrap method discussed by Peterson et al. (2004) to estimate uncertainties. IPV values of 60%-90% in 5% increments were measured, as well as the σ_{line} and FWHM. We used 5000 Monte Carlo realizations to estimate the uncertainties in each measurement. The line widths for each of the lines for each subset of data are given in Tables 1 and 2. These were then used to test the virial relationship for each parametrization. According to eq. (1), we expect $\Delta V \propto \tau^{-1/2}$. However, because the error in time lag were much greater than the errors in ΔV, we used the time lag as the dependent variable, so that our expected relation is $\tau \propto \Delta V^{-2}$. We fit the data using τ_{cent} as the time lag, and σ_{line}, FWHM, and IPV as the line

width parameter. The fits are described in Table 3. Each parametrization was force-fit to a slope of $b = -2$, and a best-fit slope was also determined. The best-fit relations were obtained using the code BCESREGRESS. We used the BCES bisector bootstrap values for our linear fits. We focused on τ_{cent} in order to be consistent with the work by Peterson et al. (2004).

6.2 RMS Spectra Behavior

The measurements from rms spectra are shown in Figure 1, along with the best fits to these data. The IPV parameter shows the expected relationship with the emission time lag. Based on the shape of the fits, it is clear that the IPV parameter yields better fits than the FWHM parameter, and is almost as good as σ_{line}. When we examine the χ^2 values for each of the fits, we see that these agree with the graphical observations. The χ^2 values for FWHM are noticably higher than the others. This is due not only to the larger scatter in the line widths, but also due to an outlier. For the rms spectra, the year 5 Hβ width was an outlying point, and when that is removed, the the χ^2 was noticably lowered. The fits with the outlier and without the outlier are shown in Figure 3.

6.2 Mean Spectra Behavior

The mean spectra fits are shown in Figure 2. The IPV parameter shows the expected relationship with the emission time lag. Based on the shape of the fits, it is clear that the IPV parameter is a better fit than the FWHM parameter, and is almost as good as σ_{line}. The χ^2 values once again agree with the graphical observations. The χ^2 values for FWHM are once again very high. The mean spectra is more susceptible to the constant flux emission. Since the widths that we want are from the reverberating regions, we really want just the variable part of the spectrum. FWHM is affected by narrow line and constant flux contamination, which means that the FWHM fits should be less precise. However, the FWHM once again has an outlying point, the CIII]λ1909 width from year 5.When this is taken out, the χ^2 values for FWHM were lowered, but were still significantly higher, as expected. The fits with the outlier and without the outlier are shown in Figure 4.

6.3 Bias of Inter-Percentile Velocity

In addition to consistency with the virial relationship, we also desire a parameter that is usable on spectra as observed, without having to use a complicated deblending process on each spectrum. This means that there should be no systematic bias in the width measurements when using deblended spectra as opposed to spectra that has blended features. If there is bias, this means we will have incorrect measurements on the high mass end of the relation. Thus, while random scatter is acceptable, any observable trend as a function of velocity constitutes a bias and is therefore unacceptable.

We used 37 spectra of NGC 5548 that spanned over a long time period. For the spectra as observed, we only removed the narrow lines (Hβ, [OIII]λ4959,5007). The fitted spectra had the

AGN continuum, the host galaxy, FeII emission, Balmer continuum emission and the narrow lines modeled out. All that was left, therefore, would be the BLR component of Hβ as well as the FeII shelf on the red side.

Due to the FeII shelf, we looked both at the bias of the parametrizations over the entire line, as well as without the shelf. The "with shelf" graphs have the line limits from the edge of the blue to the edge of the red side of the emission line, so as to include the FeII shelf. The "without shelf" graphs have defined the line limits so that the line is artificially cut off before the shelf. While this is not entirely accurate, we are using it as a rough estimation to see if including the shelf will affect the bias of the parameter. We also looked at the "IPV blue" and "σ_{line} blue" to see if the FeII shelf affected the bias of the parameter. These are measured by looking at the half-width of the blue side. This side is unaffected by the FeII shelf on the red side of the line. This means when we look at the "blue" velocity dispersion width, we should get the relation that is based purely on the emission line (Denney et al. 2009). We measured the line widths of these spectra. Then we plotted the fitted results with and without the shelf against the local continuum fit, and the residuals with respect to the width from the local continua method, as done by Denney et al. (2009). These results are shown in Figures 5-12.

Both σ_{line} and FWHM parametrizations show systematic bias. When the IPV value is close to 50%, the parameter shows bias similar to FWHM. When the IPV value is close to 100%, the parameter shows bias similar to σ_{line}. However, when the IPV value is around 65%-70%, there is no apparent systematic bias. The "without shelf" measurements show bias that is not present when the entire line is taken into account. This means that artificially cutting the data off before the shelf is not an accurate way to measure the line width, and not much can be gained from this parametrization. The "blue side" measurements shows approximately the same bias as the entire line, which means the bias does not depend on the FeII shelf.

There are outliers in all of the line width measurements. These all come from the same set of spectra, whether on the high or low end. In the case of the significantly lower outliers, the line is very broad and noisy, so that it is comparable to the noise in the continuum. For the high outliers, the line has significant flux on top of the broad line, so that the profile appears much taller than the actual broad component should be.

7. CONCLUSION

The goal of this project was to find a simple descriptor of line width that, through the reverberation mapping equation, always gives a consistent black hole mass. The IPV parametrization responds how it was expected to. At IPV values closer to 50%, the IPV parameter behaves more like FWHM. At IPV values closer to 100%, the parameter behaves more like σ_{line}. This means at all IPV values, the IPV parameter is consistent with the expected virial relationship. When we look at the bias in the parameter, at IPV values around 65%-70%, there is no apparent bias in the parameter as a function of velocity if the entire line is included in the measurement. This means that the IPV

parametrization could therefore be a good new parametrization for the line widths of the broad lines of AGN. Further testing should be done to see if the parameter is robust.

7.1 Future Work

While the FeII shelf does not seem to affect the bias of the parametrization, it obviously will affect the measurement of the line width. Therefore the next step in this project would be to isolate the Hβ line from any other spectral features that might be blending with the line, and as a result skewing our results. The most important of these features is the FeII shelf on the red side of Hβ, which can be removed using a FeII template.

The problem with FeII emission is that it does vary on scales larger than the reverberation variance. This means that the modeling and removal of FeII is not as simple as blindly applying the same FeII template to all spectra. The template by Kovačevič et al. (2010) is interesting because it has more free parameters to work with when creating the template itself. While this will allow for variance within FeII in an individual spectrum, it does make the process more involved. The next step in this project would be to look for a simple, yet sufficient method of subtracting the FeII emission.

In addition to subtracting FeII emission, the intrinsic scatter of the $log(\tau)$ vs. $log(\Delta V)$ relationship should be examined. While all the parameters have that intrinsic scatter, it is most clearly seen with FWHM. All of the FWHM plots have significantly higher χ^2 values, as well as larger errors. What we are observing is that there is considerable intrinsic scatter in the $log(\tau)$ vs. $log(\Delta V)$ relationship. More detailed calculations on the fits of FWHM, as well as the other parametrizations, should be used to calculate this intrinsic scatter and its effects on how robust the parameter is.

References

Blandford, R.D., & McKee, C.F. 1982, ApJ, 255, 419

Boroson, T.A., & Green, R.F. 1992, ApJS, 80, 109

Denney, K.D., et al. 2009, ApJ, 692, 246

Kovačevič, J., et al. 2010, ApJS, 189, 15

Maoz, D., & Netzer, H. 1989, MNRAS, 236, 21

Peterson, B.M., et al. 2004, ApJ, 613, 682

Vestergaard, M. & Peterson, B.M. 2005, ApJ, 625, 688

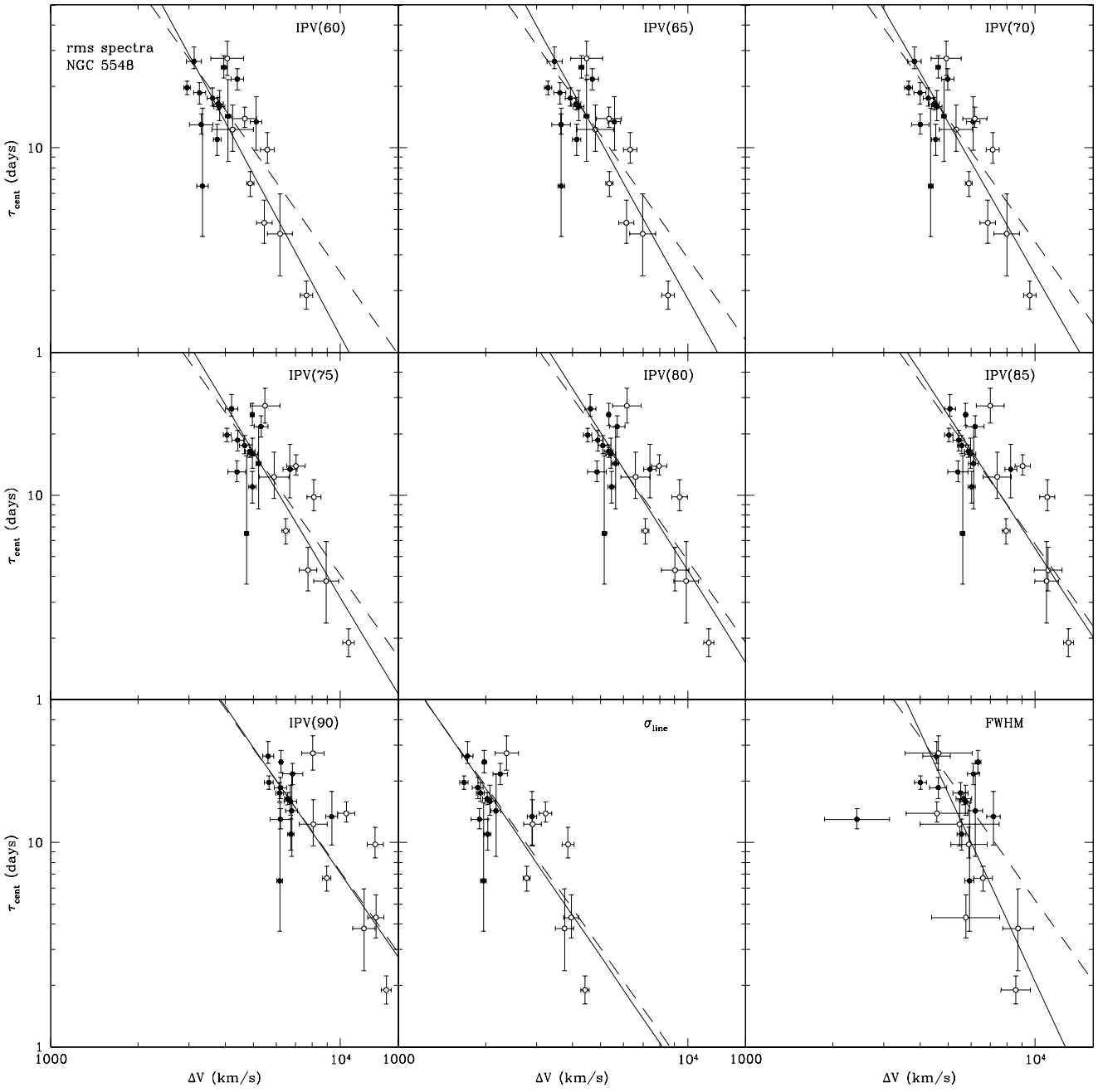

Fig. 1.— Virial relationship fits of rms spectra for all IPV of values 60%-90% in 5% increments, σ_{line}, and FWHM. The solid line is the forced fit, and the dashed line is the best fit slope. The plotted FWHM fits are calculated with the outlier.

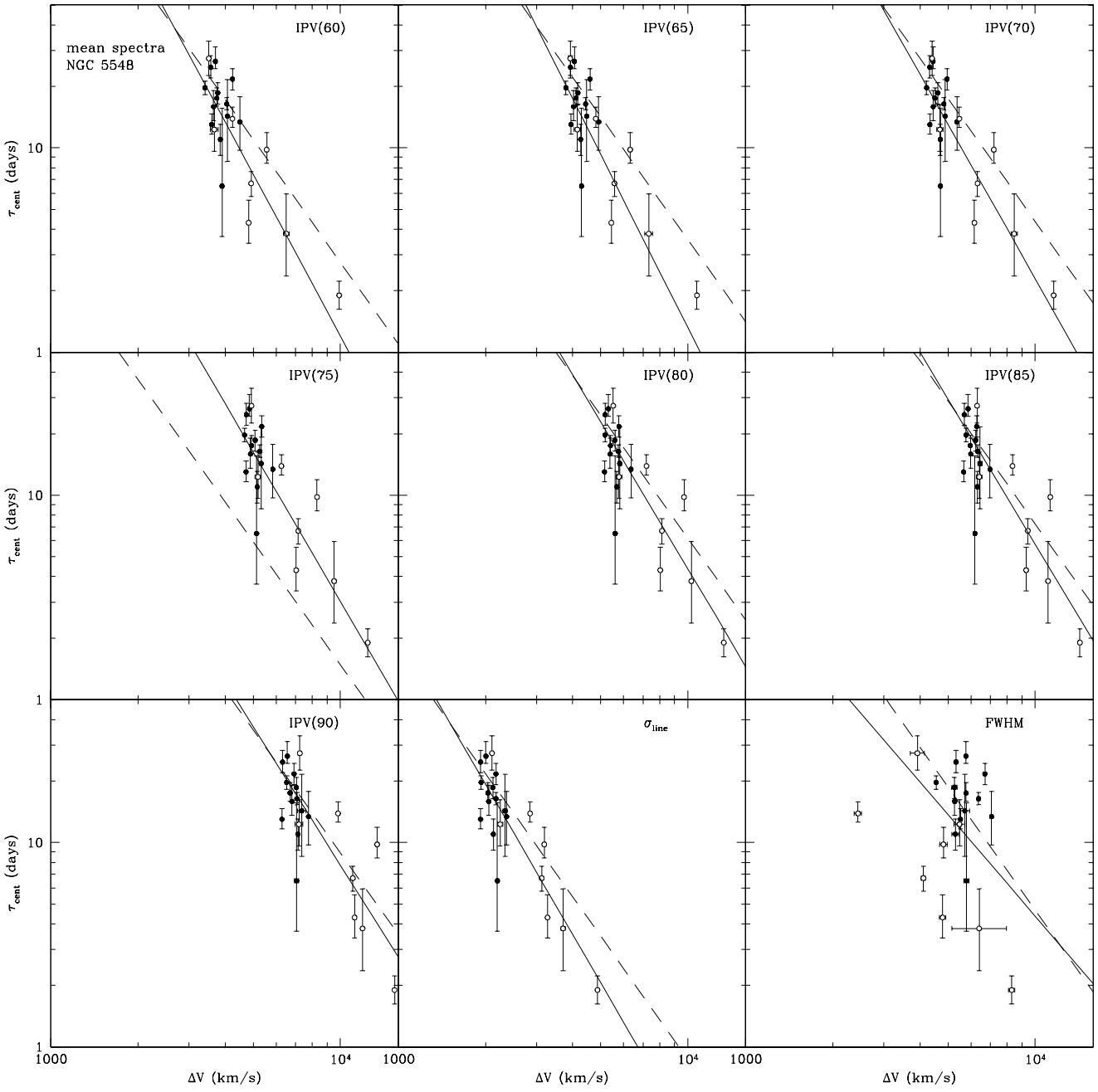

Fig. 2.— Virial relationship fits of mean data for all IPV of values 60%-90% in 5% increments, σ_{line}, and FWHM. The solid line is the forced fit, and the dashed line is the best fit slope. The plotted FWHM fits are calculated with the outlier.

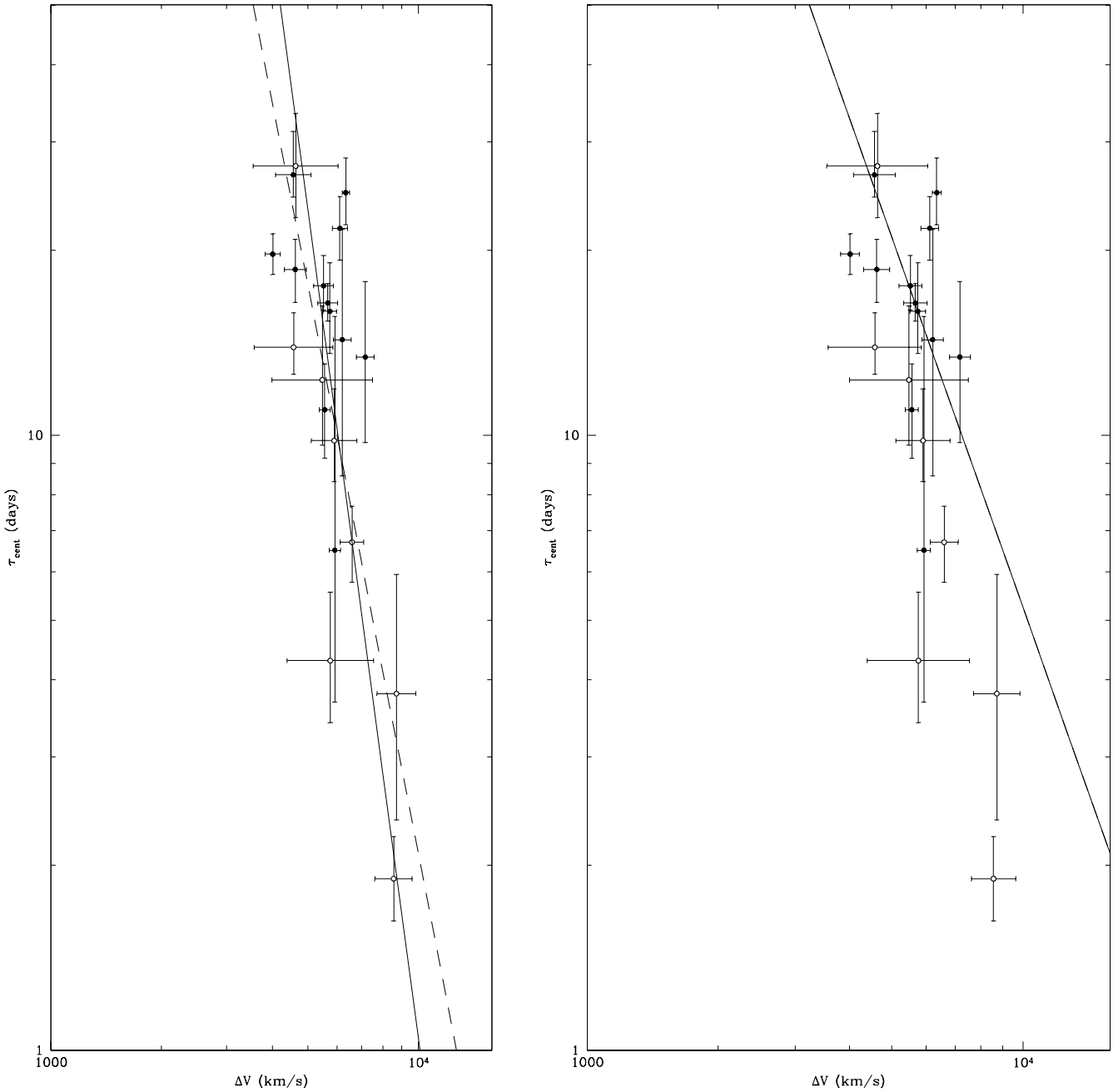

Fig. 3.— Virial relationship fits of rms data for FWHM. Left: Best fits. The dotted line is the fit calculated with the outlier, and the solid line is the fit calculated without the outlier. Right: Forced fits. The dotted line is the fit calculated with the outlier, and the solid line is the fit calculated without the outlier.

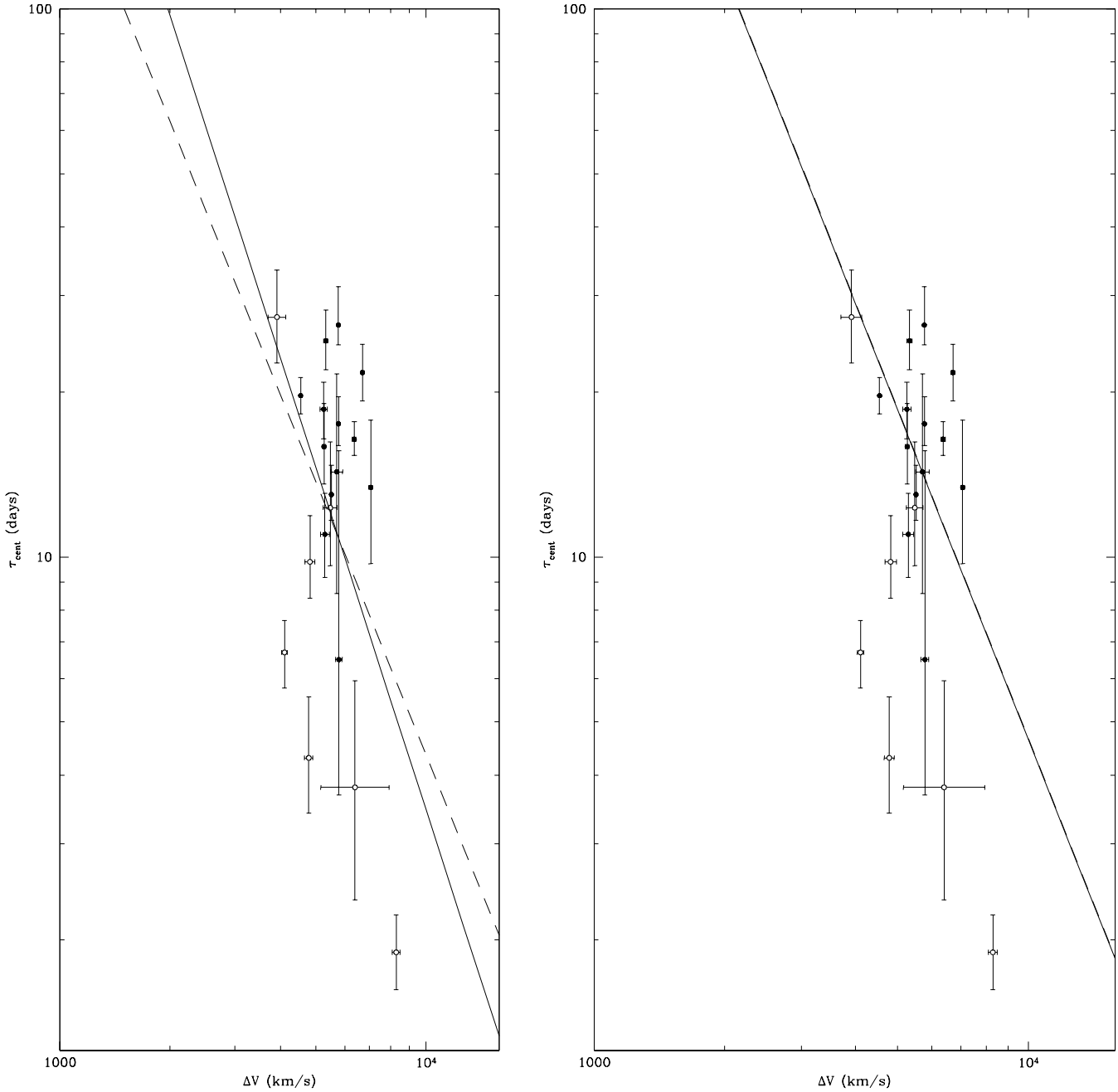

Fig. 4.— Virial relationship fits of mean data for FWHM. Left: Best fits. The dotted line is the fit calculated with the outlier, and the solid line is the fit calculated without the outlier. Right: Forced fits. The dotted line is the fit calculated with the outlier, and the solid line is the fit calculated without the outlier.

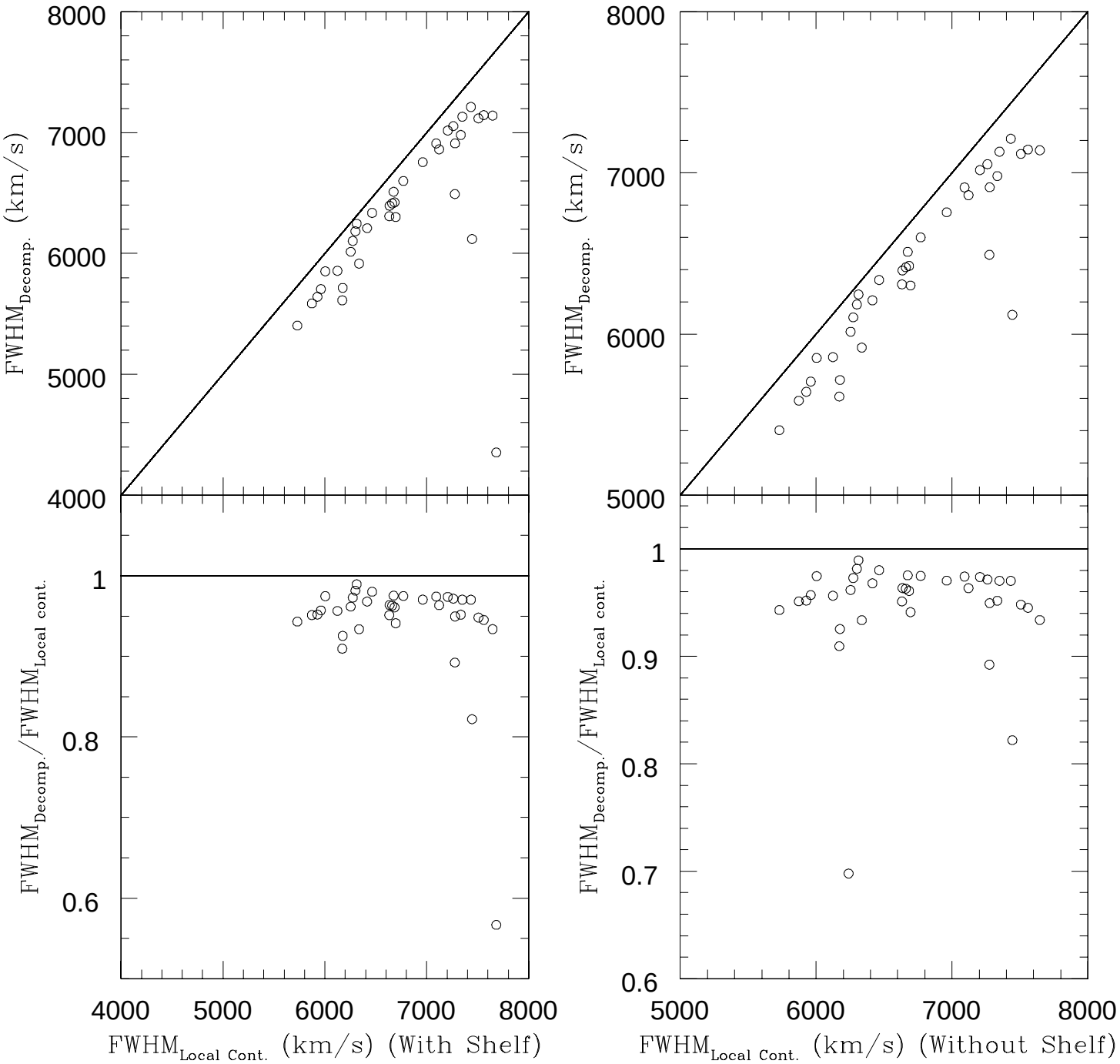

Fig. 5.— Bias of FWHM. The systematic bias is seen in the slight curvature in the data. The outlier is from an emission line with very low flux, comparable to the continuum.

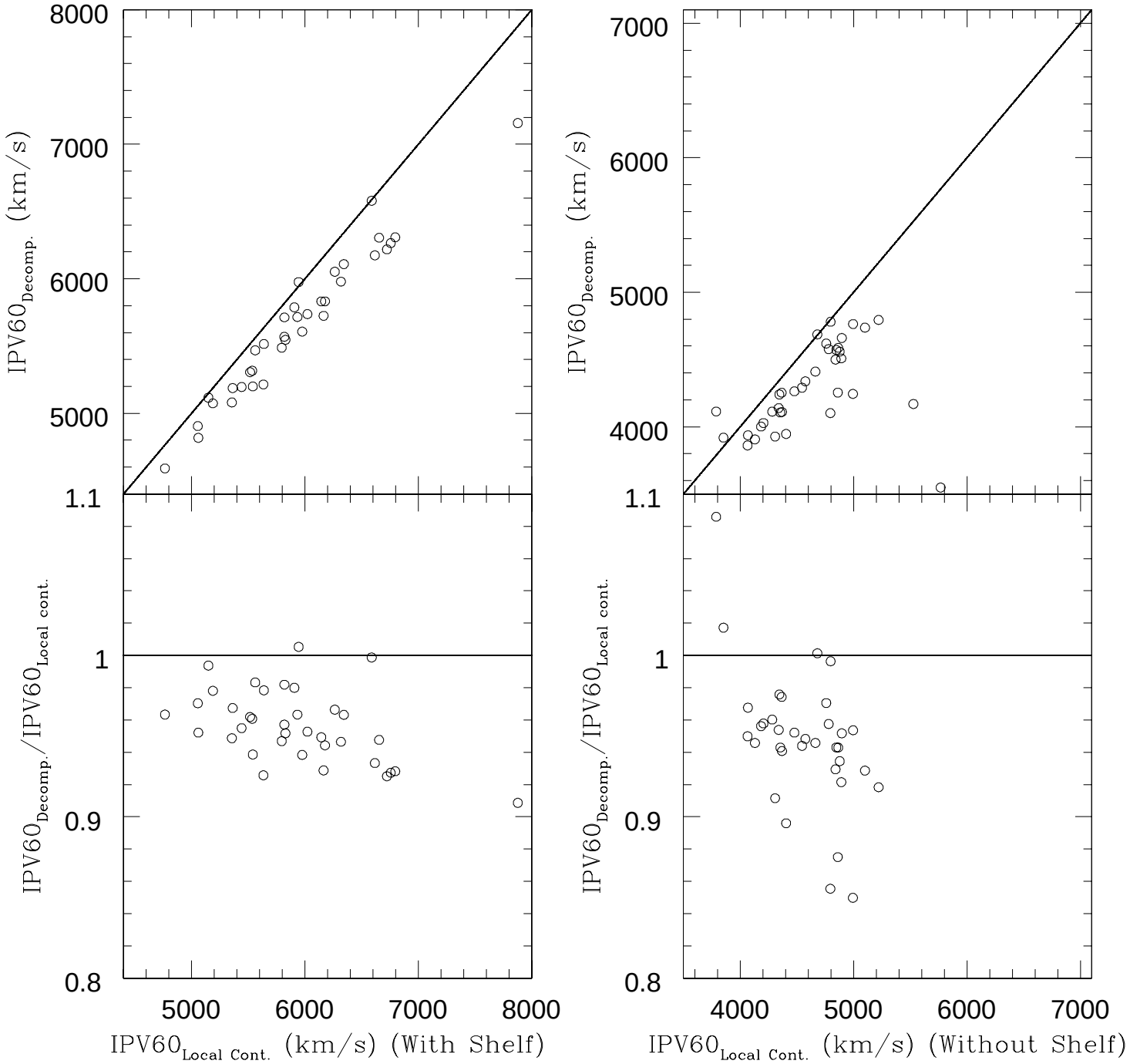

Fig. 6.— Bias of $IPV(60)$. The shape of the data trend is similar to the FWHM parametrization. The lower outlier is from an emission line with very low flux, comparable to the continuum. The high outliers have excess flux on top of the broad line component of Hβ, skewing the line width measurement.

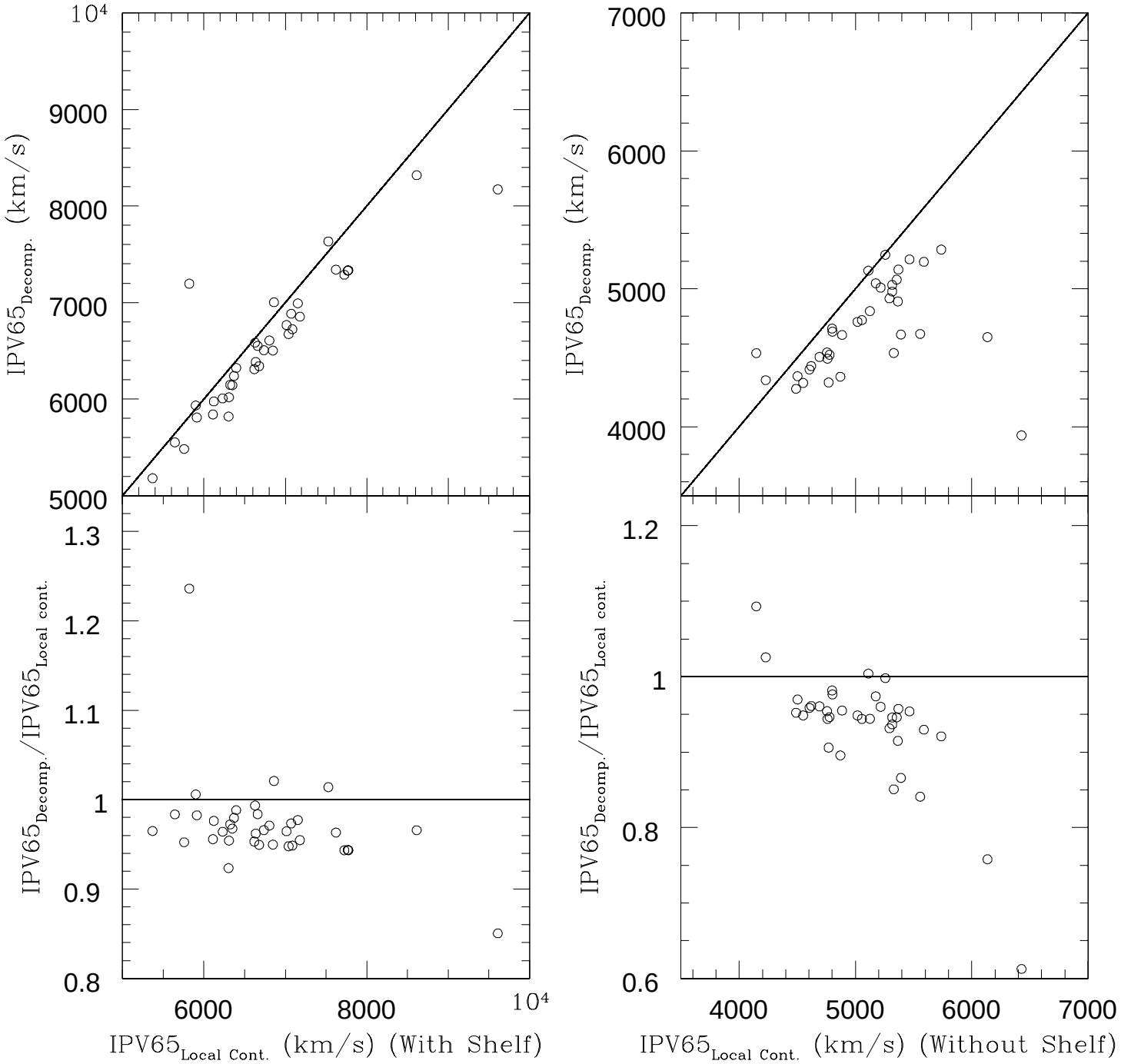

Fig. 7.— Bias of $IPV(65)$. This has no systematic bias in the graph with the shelf, just a constant offset which can be corrected for. The lower outliers are from emission lines with very low flux, comparable to the continuum. The high outliers have excess flux on top of the broad line component of Hβ, skewing the line width measurement. The graph without the shelf shows systematic bias because a large part of the line profile is ignored in that calculation.

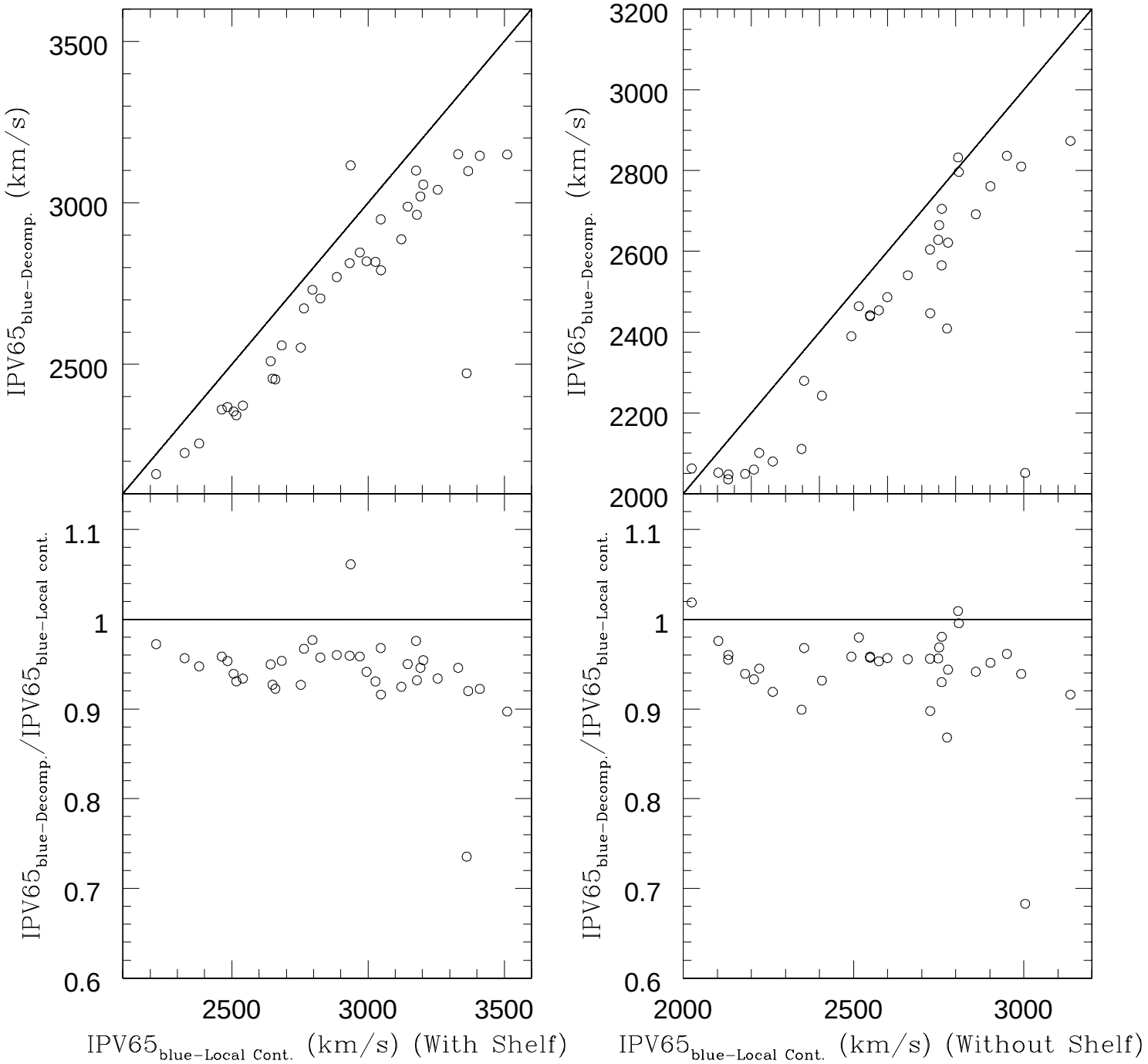

Fig. 8.— Bias of $IPV(65)_{blue}$. The trend is similar to $IPV(65)$, when the shelf is included. This relation was seen for every IPV_{blue} value. Due to the artificial cutoff for the graph without the shelf, we do not expect an exact correlation in that relation. The lower outliers are from emission lines with very low flux, comparable to the continuum. The high outlier have excess flux on top of the broad line component of Hβ, skewing the line width measurement.

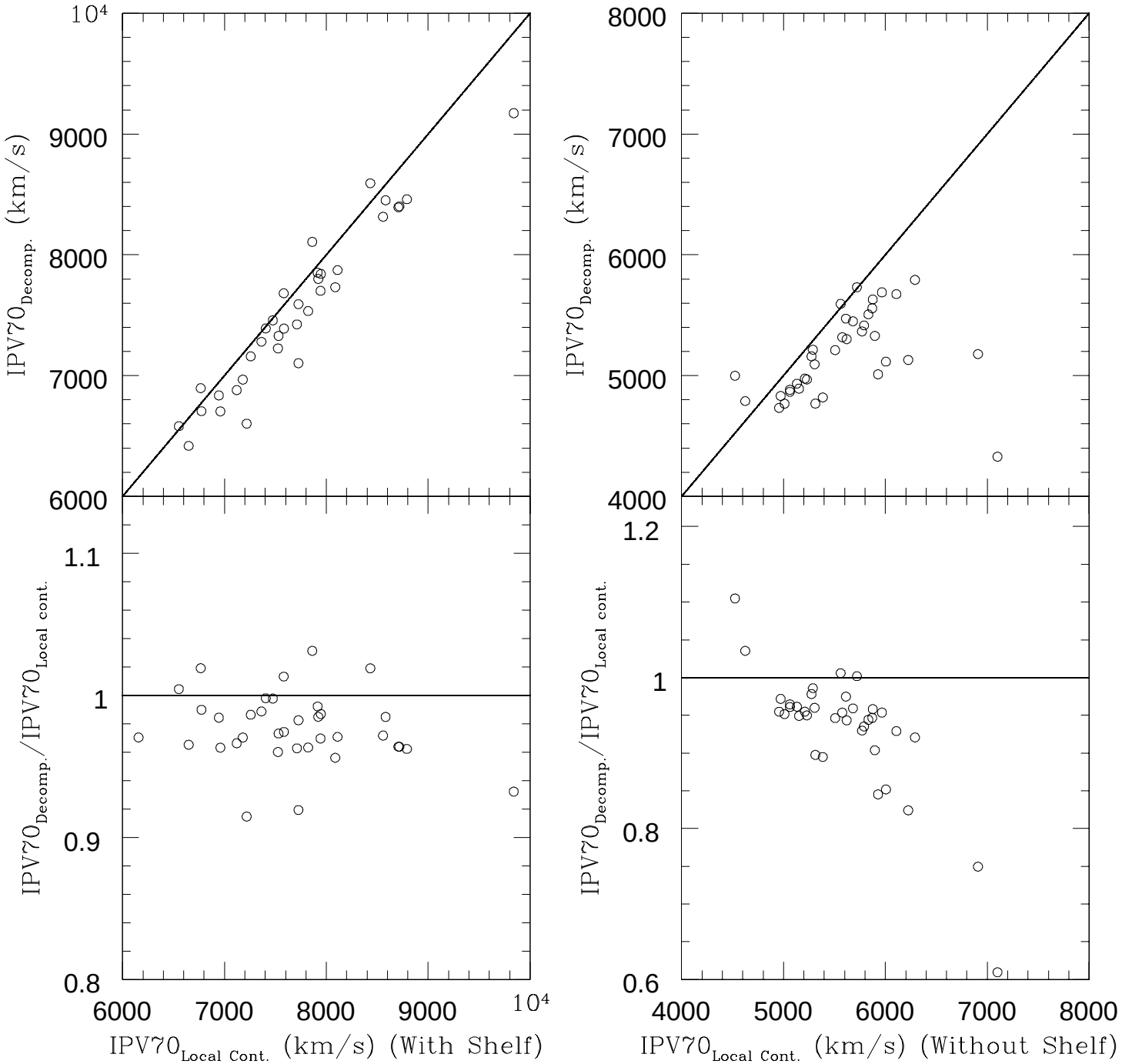

Fig. 9.— Bias of $IPV(70)$. This has no systematic bias, and seems to center around the 1:1 line. The lower outliers are from emission lines with very low flux, comparable to the continuum.

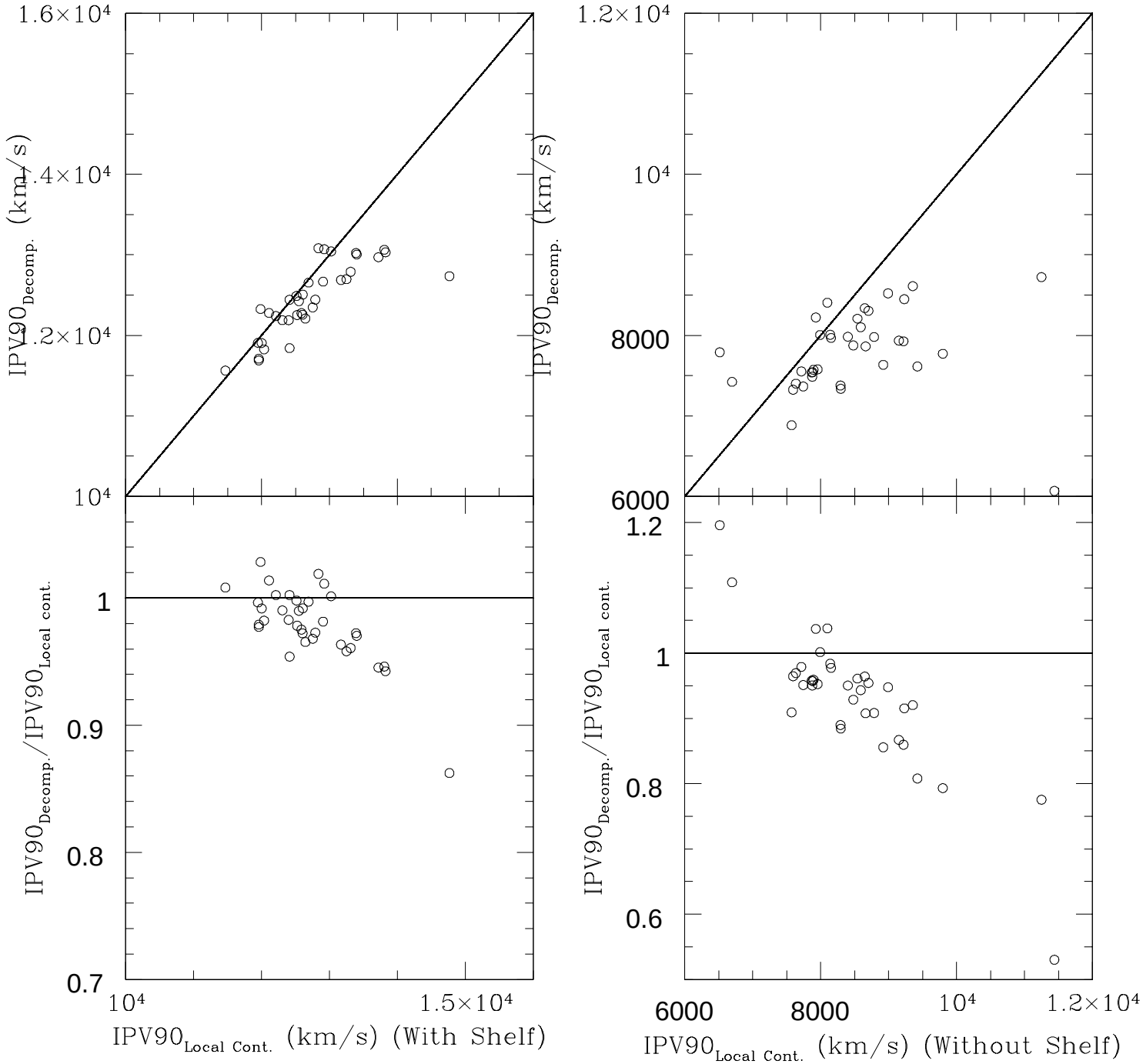

Fig. 10.— Bias of $IPV(90)$. There is clear systematic bias, and does not correlate at all with the 1:1 line. The lower outliers are from emission lines with very low flux, comparable to the continuum.

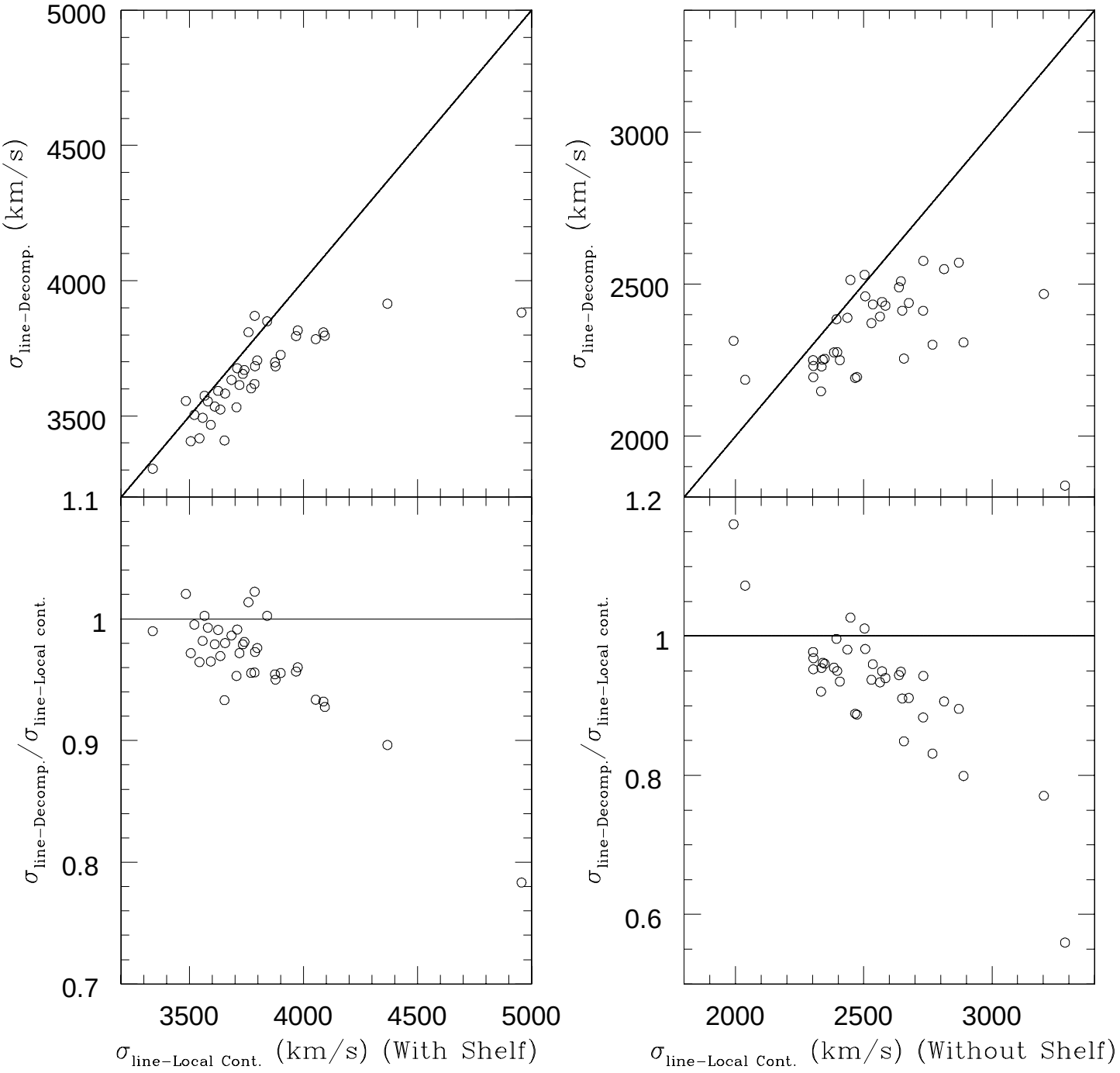

Fig. 11.— Bias of σ_{line}. The systematic bias is similar to that of $IPV(90)$. The lower outliers are from emission lines wdth very low flux, comparable to the continuum.

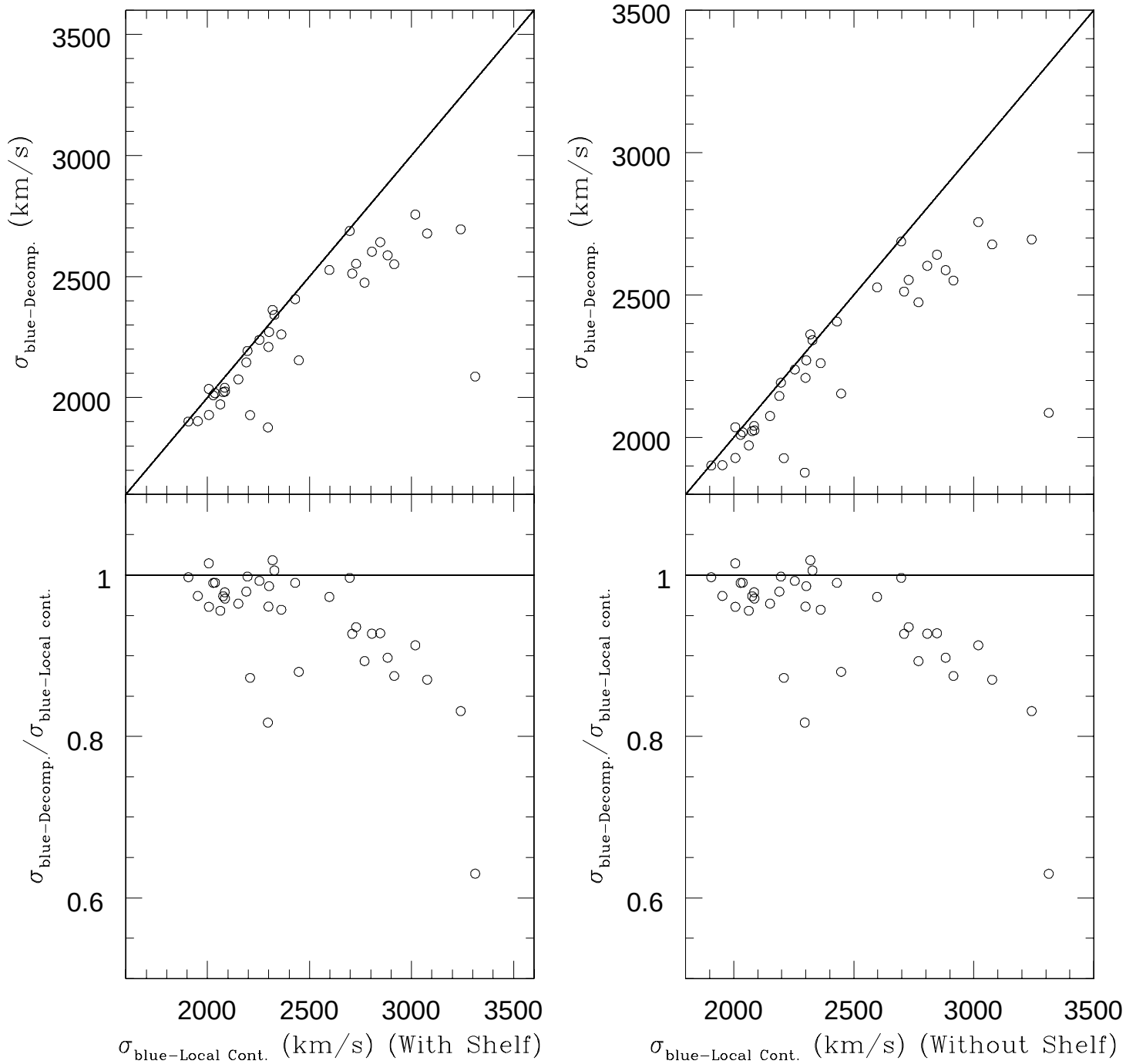

Fig. 12.— Bias of σ_{blue}. The systematic bias is similar to that of σ_{line}, but with increased scatter. The lower outlier is from an emission line with very low flux, comparable to the continuum.

Table 1. Rest-Frame Lag and Line Widths of the rms spectra for NGC 5548

Line (1)	τ_{cent}[1] (days) (2)	IPV(60) (km s^{-1}) (3)	IPV(65) (km s^{-1}) (4)	IPV(70) (km s^{-1}) (5)	IPV(75) (km s^{-1}) (6)	IPV(80) (km s^{-1}) (7)	IPV(85) (km s^{-1}) (8)	IPV(90) (km s^{-1}) (9)	σ_{line} (km s^{-1}) (10)	FWHM (km s^{-1}) (11)
Hβ	$19.7^{+1.5}_{-1.5}$	2954±78	3286±95	3651±109	4058±126	4511±150	5033±164	5660±191	1688±56	4014±196
Hβ	$18.6^{+2.1}_{-2.3}$	3263±158	3614±172	4000±188	4416±202	4887±218	5441±244	6203±305	1880±82	4623±319
Hβ	$15.9^{+2.9}_{-2.5}$	3821±168	4196±177	4577±187	4973±192	5421±215	5966±267	6725±332	2073±82	5742±238
Hβ	$11.0^{+1.9}_{-2.0}$	3756±122	4132±132	4530±142	4967±148	5455±155	6028±166	6743±165	2034±52	5563±191
Hβ	$13.0^{+1.6}_{-1.4}$	3306±311	3652±271	4010±279	4393±311	4856±363	5408±431	6208±519	1908±126	2421±626
Hβ	$13.4^{+3.8}_{-4.3}$	5120±234	5575±277	6100±332	6699±371	7399±378	8232±402	9328±438	2895±111	7170±394
Hβ	$21.7^{+2.6}_{-2.6}$	4402±219	4678±235	4985±249	5318±287	5700±351	6194±449	6841±551	2250±131	6116±289
Hβ	$16.4^{+1.2}_{-1.1}$	3783±155	4111±164	4474±181	4868±191	5329±191	5877±185	6580±174	2026±69	5666±349
Hβ	$17.5^{+2.0}_{-1.6}$	3617±148	3929±162	4272±175	4665±186	5085±183	5568±186	6164±193	1922±60	5520±337
Hβ	$26.5^{+4.3}_{-2.2}$	3122±186	3466±204	3824±204	4207±206	4608±206	5074±216	5630±242	1734±76	4565±503
Hβ	$24.8^{+3.2}_{-3.0}$	3960±91	4290±84	4618±78	4963±72	5332±70	5749±70	6234±85	1981±30	6346±147
Hβ	$6.5^{+5.7}_{-3.7}$	3338±152	3655±95	4358±82	4742±77	5153±86	5614±99	6170±141	1968±43	5926±209
Hβ	$14.3^{+5.9}_{-7.3}$	4095±89	4465±92	4836±95	5216±107	5623±151	6124±239	6783±320	2173±87	6209±353
SiIVλ1400	$12.3^{+3.4}_{-3.0}$	4244±699	4791±704	5334±704	5902±703	6603±767	7388±829	8063±897	2908±205	5478±1725
CIVλ1549	$9.8^{+1.9}_{-1.5}$	5592±305	6323±342	7129±376	8099±447	9368±590	11004±672	13197±842	3857±181	5901±849
HeIIλ1640	$3.8^{+1.7}_{-1.8}$	6189±614	6987±723	7969±808	8928±875	9867±975	10941±1028	12066±1068	3752±273	8718±1066
CIII]λ1909	$27.4^{+5.4}_{-5.3}$	4067±531	4472±567	4931±590	5492±646	6156±701	6993±771	8038±718	2366±221	4636±1240
SiIVλ1400	$4.3^{+1.1}_{-1.0}$	5454±337	6131±362	6854±420	7729±552	9038±987	11091±1236	13259±846	3957±243	5758±1558
CIVλ1549	$6.7^{+0.9}_{-1.0}$	4885±133	5360±147	5895±160	6478±182	7135±201	7926±246	8974±304	2777±77	6599±490
HeIIλ1640	$1.9^{+0.3}_{-0.3}$	7635±378	8545±436	9570±468	10668±467	11087±467	13025±501	14402±589	4414±149	8564±1007
CIII]λ1909	$3.9^{+1.8}_{-0.4}$	4675±447	5346±528	6184±598	7024±514	7956±491	9049±553	10479±721	3227±163	4575±1126

[1]Time Lag from Peterson et al. 2004.

Table 2. Rest-Frame Lag and Line Widths of the mean spectra for NGC 5548

Line (1)	τ_{cent}[1] (days) (2)	IPV(60) (km s^{-1}) (3)	IPV(65) (km s^{-1}) (4)	IPV(70) (km s^{-1}) (5)	IPV(75) (km s^{-1}) (6)	IPV(80) (km s^{-1}) (7)	IPV(85) (km s^{-1}) (8)	IPV(90) (km s^{-1}) (9)	σ_{line} (km s^{-1}) (10)	FWHM (km s^{-1}) (11)
Hβ	$19.7^{+1.5}_{-1.5}$	3407±15	3794±17	4213±18	4668±20	5176±21	5769±23	6521±25	1932±7	4546±20
Hβ	$18.6^{+2.1}_{-2.3}$	3769±42	4172±45	4607±49	5075±50	5598±53	6226±57	7047±62	2120±19	5256±114
Hβ	$15.9^{+2.9}_{-2.5}$	3648±18	4032±19	4441±19	4888±20	5389±22	5987±25	6800±32	2052±7	5265±52
Hβ	$11.0^{+1.9}_{-2.0}$	3849±30	4264±35	4701±35	5165±38	5690±45	6315±47	7134±54	2129±14	5294±152
Hβ	$13.0^{+1.6}_{-1.4}$	3594±15	3951±15	4325±15	4723±16	5157±16	5658±19	6286±24	1924±8	5517±15
Hβ	$13.4^{+3.8}_{-4.3}$	4498±20	4924±22	5367±23	5842±26	6366±29	6981±33	7762±37	2366±10	7064±72
Hβ	$21.7^{+2.6}_{-2.6}$	4239±19	4592±19	4959±19	5351±20	5783±22	6282±23	6916±25	2174±9	6706±63
Hβ	$16.4^{+1.2}_{-1.1}$	4052±14	4434±15	4836±16	5271±17	5755±19	6327±21	7082±24	2175±6	6369±72
Hβ	$17.5^{+2.0}_{-1.6}$	3742±14	4111±16	4505±17	4931±19	5405±22	5966±26	6701±30	2039±6	5770±16
Hβ	$26.5^{+4.3}_{-2.2}$	3701±11	4059±11	4439±11	4853±12	5314±12	5860±14	6557±16	2008±5	5764±23
Hβ	$24.8^{+3.2}_{-3.0}$	3562±25	3931±25	4318±24	4731±22	5180±20	5690±18	6312±17	1924±7	5328±74
Hβ	$6.5^{+5.7}_{-3.7}$	3902±38	4293±38	4702±40	5135±40	5613±48	6190±64	7056±113	2199±24	5783±117
Hβ	$14.3^{+5.9}_{-7.3}$	4072±34	4472±37	4884±44	5325±58	5821±79	6454±107	7357±234	2339±40	5711±207
SiIVλ1400	$12.3^{+3.4}_{-3.0}$	3669±113	4155±113	4686±111	5192±117	5783±137	6406±149	7194±219	2248±47	5479±238
CIVλ1549	$9.8^{+1.9}_{-1.5}$	5565±49	6324±58	7196±69	8302±88	9699±102	11268±106	13394±126	3193±32	4820±146
HeIIλ1640	$3.8^{+1.7}_{-1.8}$	6501±150	7333±232	8460±211	9510±136	10285±126	11074±126	11925±146	3708±58	6401±1379
CIII]λ1909	$27.4^{+5.4}_{-5.3}$	3511±37	3925±43	4404±49	4929±50	5524±60	6298±65	7241±86	2107±19	3917±217
SiIVλ1400	$4.3^{+1.1}_{-1.0}$	4822±36	5445±40	6164±44	7035±53	8035±60	9301±100	11198±141	3277±27	4786±125
CIVλ1549	$6.7^{+0.9}_{-1.0}$	4918±12	5583±12	6316±12	7157±15	8140±20	9428±30	11038±32	3130±7	4108±70
HeIIλ1640	$1.9^{+0.3}_{-0.3}$	9904±48	10750±43	11578±44	12431±42	13312±43	14261±51	15379±62	4875±19	8293±196
CIII]λ1909	$3.9^{+1.8}_{-0.4}$	4237±17	4811±21	5470±23	6257±26	7198±30	8346±32	9814±41	2852±11	2442±71

[1]Time Lag from Peterson et al. 2004.

Table 3. Virial Relationship Fits

Data Set	Free Slope			Fixed Slope $b = -0.5$	
	a	b	χ^2	a	χ^2
(1)	(2)	(3)	(4)	(5)	(6)
NGC 5548: RMS					
$\tau_{\rm cent}$ vs. $\sigma_{\rm line}$	8.10 ± 1.19	-2.07 ± 0.35	9.04	7.88 ± 0.01	8.78
τcent vs. FWHM	12.60 ± 7.27	-3.07 ± 1.93	36.79[1]	8.72 ± 0.02	25.82[2]
$\tau_{\rm cent}$ vs. IPV(60)	10.60 ± 1.65	-2.63 ± 0.45	9.40	8.39 ± 0.02	7.98
$\tau_{\rm cent}$ vs. IPV(65)	10.50 ± 1.39	-2.56 ± 0.38	8.92	8.46 ± 0.02	7.38
$\tau_{\rm cent}$ vs. IPV(70)	10.30 ± 1.40	-2.48 ± 0.38	8.52	8.54 ± 0.01	7.24
$\tau_{\rm cent}$ vs. IPV(75)	9.98 ± 1.32	-2.37 ± 0.35	8.23	8.61 ± 0.01	7.21
$\tau_{\rm cent}$ vs. IPV(80)	9.59 ± 1.51	-2.24 ± 0.40	8.07	8.68 ± 0.01	7.45
$\tau_{\rm cent}$ vs. IPV(85)	9.42 ± 1.28	-2.17 ± 0.33	8.42	8.76 ± 0.01	8.02
$\tau_{\rm cent}$ vs. IPV(90)	9.05 ± 0.15	-2.05 ± 0.39	8.98	8.86 ± 0.01	8.72
NGC 5548: Mean[3]					
$\tau_{\rm cent}$ vs. $\sigma_{\rm line}$	9.34 ± 0.79	-2.44 ± 0.23	5.04	7.94 ± 0.01	4.97
$\tau_{\rm cent}$ vs. FWHM	7.24 ± 6.0	-1.65 ± 1.60	29.74[4]	8.667 ± 0.01	29.84[5]
$\tau_{\rm cent}$ vs. IPV(60)	10.60 ± 1.72	-2.63 ± 0.48	6.94	8.44 ± 0.01	5.38
$\tau_{\rm cent}$ vs. IPV(65)	11.40 ± 2.28	-2.82 ± 0.63	7.44	8.55 ± 0.01	5.58
$\tau_{\rm cent}$ vs. IPV(70)	10.40 ± 1.53	-2.51 ± 0.42	5.47	8.64 ± 0.01	5.56
$\tau_{\rm cent}$ vs. IPV(75)	10.20 ± 1.29	-2.43 ± 0.34	5.93	8.72 ± 0.01	5.42
$\tau_{\rm cent}$ vs. IPV(80)	10.20 ± 1.34	-2.39 ± 0.35	4.96	8.79 ± 0.01	5.26
$\tau_{\rm cent}$ vs. IPV(85)	10.20 ± 1.22	-2.36 ± 0.32	5.61	8.86 ± 0.01	5.27
$\tau_{\rm cent}$ vs. IPV(90)	9.89 ± 1.43	-2.25 ± 0.37	6.53	8.95 ± 0.01	5.92

[1]a $= 17.9 \pm 8.37$, b $= -4.47 \pm 2.23$, $\chi^2 = 27.32$ when the Hβ width for year 5 is removed.

[2]a $= 8.7 \pm 0.02$, and $\chi^2 = 13.59$ when the Hβ width for year 5 is removed.

[3]Narrow component of Hβ removed.

[4]a $= 8.8 \pm 8.22$, b $= -2.07 \pm 2.20$, $\chi^2 = 27.77$ when the CIII]λ1909 width for year 5 is removed.

[5]a $= 8.669 \pm 0.01$, and $\chi^2 = 21.63$ when the CIII]λ1909 width for year 5 is removed.